nature physics

LETTERS

PUBLISHED ONLINE: 17 JUNE 2012 | DOI: 10.1038/NPHYS2348

Density functional theory for atomic Fermi gases

Ping Nang Ma[1], Sebastiano Pilati[1,2], Matthias Troyer[1]* and Xi Dai[3]

The interplay between interaction and inhomogeneity for electrons in solids generates many interesting phenomena, including insulating and metallic behaviour, magnetism, superconductivity, quantum criticality and more exotic phases[1]. Many of the same phenomena appear in ultracold fermionic atoms in optical lattices[2], which provide clean, controlled and tunable 'quantum simulators' to explore the intriguing physics of fermionic systems. Although density functional theory[3–5] (DFT) is widely used to calculate material properties[6], it has not yet been applied to cold atomic gases in optical lattices. Here we present a new density functional for short-range interactions (as opposed to Coulomb interactions of electrons), which renders DFT suitable for atomic Fermi gases. This grants us access to an extensive toolset, previously developed for materials simulations, to calculate the static and dynamic properties of atomic Fermi gases in optical lattices and external potentials. Ultracold atom quantum simulators can in turn be used to explore limitations of DFT functionals, and to further improve hybrid functionals, thus forming a bridge between materials simulations and atomic physics.

Ultracold atomic gases have several advantages over materials for systematically exploring fermionic quantum systems. In materials, strong interactions go hand in hand with increasing localization of electrons as one moves from weakly correlated materials with *s* and *p* electrons to transition metal compounds with *d* electrons, and lanthanides and actinides with even more localized *f* orbitals. In contrast, all relevant parameters can be almost arbitrarily changed for fermionic gases in optical lattices: increasing the intensity of the optical lattice tunes continuously from shallow lattices with extended wave functions to deep lattices with almost localized Wannier functions, and the band structure can be further modified by changing the laser wave form. The strength of the inter-atomic interactions can independently be varied by tuning an external magnetic field across Feshbach resonances[7]. This facilitates a controlled realization of intriguing quantum phenomena in fermionic systems, and the systematic exploration of interaction and localization effects. The simplicity of atomic gases, the absence of core electrons and the ability to realize strongly interacting systems already in the lowest band makes optical lattice systems also much easier to treat from a theoretical point of view, avoiding the need for expensive all-electron calculations including the core electrons or the use of less reliable pseudopotentials incorporating their effects.

So far, the experimental and theoretical focus has been on deep optical lattices, which are described well by single-band Hubbard models and where exciting progress has been achieved. In experiments, a Mott insulating phase has been realized[8,9], and the detection of a Néel state seems feasible in the not too distant future. Progress in simulation methods[10,11] now allows one to accurately simulate the Hubbard model in the same temperature regime[12], thus enabling direct comparison between experiments and simulation for the fermionic Hubbard model similar to what has previously been done for bosons[13].

Even more intriguing physics than in the Hubbard model is expected in shallow optical lattices, where—in analogy to materials—a rich variety of phases is expected as the bandgap closes and multi-band and orbital effects become important. Although shallow lattices are easy to achieve experimentally by reducing the laser amplitude, they pose a challenge to theoretical treatments. As the bandgap is reduced a single-band description fails and there are fundamental problems for deriving reliable multi-band Hubbard type models[14]. We thus propose to investigate this largely unexplored regime using DFT with a new exchange correlation functional for atomic quantum gases. As a first application we will focus on the competition between paramagnetic, ferromagnetic and antiferromagnetic (AF) phases. Specifically, we will show that the ferromagnetic phase of repulsively interacting fermions, which was investigated in experiment[15] and in simulations[16], is substantially enlarged in an optical lattice and a non-trivial phase diagram is obtained owing to band structure effects.

DFT is the workhorse for electronic structure simulations and has been widely and highly successfully used for many decades[6]. Although there are open challenges in calculating spectral properties of strongly correlated systems, DFT works extremely well in the weakly correlated regime and gives accurate ground state energies and densities also in the presence of strong correlations. Following Hohenberg and Kohn[3] (HK), the exact ground-state energy E and ground state density ρ can be determined by minimizing an energy functional of the density:

$$E[\rho] = \int \mathrm{d}\mathbf{r}\, V(\mathbf{r})\rho(\mathbf{r}) + F[\rho]$$

where the first term is the potential energy due to the external potential $V(\mathbf{r})$ at location $\mathbf{r}$. In the context of materials $V(\mathbf{r})$ is the electrostatic potential (pseudopotential) of nuclei (and core electrons), whereas in ultracold atomic gases $V(\mathbf{r})$ is the optical lattice potential (see Methods). The second term is an unknown but universal functional F which includes the interaction and kinetic energies, but does not explicitly depend on $V(\mathbf{r})$. Generalizing to potentially spin-polarized systems one introduces separate densities of the two spin components $\rho_\uparrow$ and $\rho_\downarrow$:

$$E[\rho_\uparrow, \rho_\downarrow] = \int \mathrm{d}\mathbf{r}\, V(\mathbf{r})[\rho_\uparrow(\mathbf{r}) + \rho_\downarrow(\mathbf{r})] + F[\rho_\uparrow, \rho_\downarrow] \qquad (1)$$

An explicit (but rather inaccurate) expression for $F[\rho_\uparrow, \rho_\downarrow]$ is given by the HK-local spin density approximation[3] (LSDA)

$$F[\rho_\uparrow, \rho_\downarrow] = \int \mathrm{d}\mathbf{r}\, \epsilon(\rho_\uparrow(\mathbf{r}), \rho_\downarrow(\mathbf{r}))$$

where $\epsilon(\rho_\uparrow, \rho_\downarrow)$ is the ground-state energy density of a homogeneous Fermi gas with the given spin densities. The Thomas–Fermi approximation is recovered as a mean-field approximation

[1]Theoretische Physik, ETH Zurich, 8093 Zurich, Switzerland, [2]The Abdus Salam International Centre for Theoretical Physics, 34014 Trieste, Italy, [3]Institute of Physics, Chinese Academy of Science, Beijing 100190, China. *e-mail: troyer@phys.ethz.ch.

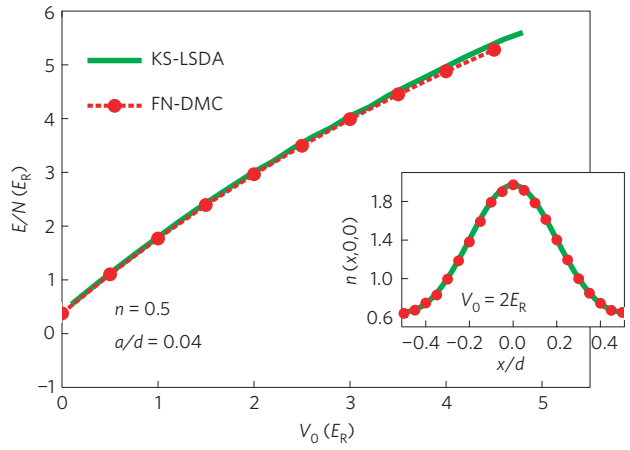

Figure 1 | Comparison of DFT results to QMC. Energy per particle E/N versus optical lattice intensity V_0, at quarter-filling $n = \rho d^3 = 0.5$, with scattering length $a = 0.04d$. The green curve plots the results of KS DFT within the LSDA, the red points show fixed-node diffusion Monte Carlo simulations. Inset: cross-sectional density profile on one lattice site, at a particular lattice intensity of $V_0 = 2.0E_R$.

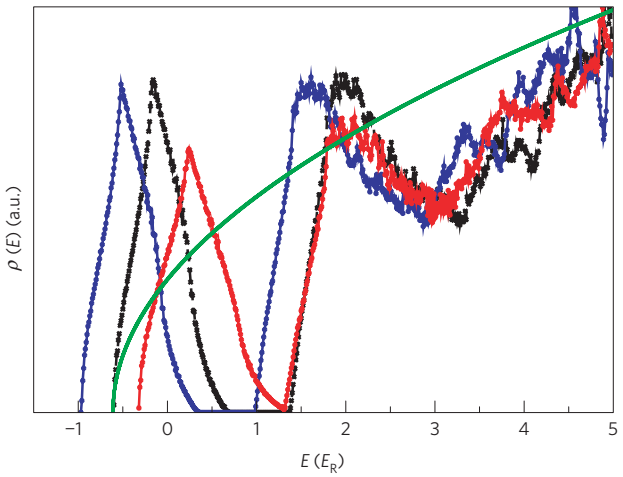

Figure 2 | Density of states. Results of KS DFT calculations at half-filling $n = \rho d^3 = 1$ with optical lattice intensity $V_0 = 3E_R$ and scattering length $a = 0.12d$ are shown indicated by the blue (red) symbols for the majority (minority) spin component. The density of states of the interacting gas is compared against that of non-interacting species (black crosses) and that obtained in the HK-LSDA method (green line), which shows no bandgap. The Fermi level is at $E = 0$.

for $\epsilon(\rho_\uparrow, \rho_\downarrow)$. A better approximation is to use the results of a quantum Monte Carlo (QMC) simulation with the given density (see Methods). Although in the quantum gases community this is referred to as the 'local density approximation' (LDA), we will explicitly call it the HK-LSDA, to avoid confusion with the common use of 'LDA' in electronic structure calculations.

The kinetic part is usually highly non-local and cannot be treated well under the local approximation. Therefore, Kohn and Sham[4] (KS) proposed a more accurate functional by explicitly including the exact kinetic energy T_0 of non-interacting fermions. What is left is the interaction energy E_{HXC}, combining the usual Hartree (mean-field term) E_{H} and the exchange–correlation correction E_{XC}:

$$F[\rho_\uparrow, \rho_\downarrow] = T_0[\rho_\uparrow, \rho_\downarrow] + E_{\mathrm{HXC}}[\rho_\uparrow, \rho_\downarrow]$$

A simple yet often reliable treatment of E_{HXC} is the LSDA

$$E_{\mathrm{HXC}}[\rho_\uparrow, \rho_\downarrow] = \int \mathrm{d}\mathbf{r}\, \epsilon_{\mathrm{HXC}}(\rho_\uparrow(\mathbf{r}), \rho_\downarrow(\mathbf{r}))$$

where the functional is replaced by an integral over the interaction energy of a uniform system with the same local density. For contact interactions, and unlike the Coulomb case, the Hartree term depends only on the local densities, and we can thus combine it with the exchange–correlation terms into one interaction energy term ϵ_{HXC}. We will refer to this functional explicitly as the KS-LSDA functional.

The LSDA functionals have been obtained using fixed-node diffusion Monte Carlo simulations, similar to previous calculations for the 3D electron gas[17]. In the Supplementary Information we report an explicit parametrization of this functional which accurately fits the QMC results for the energy density and reproduces the known behaviour in the limiting cases of small coupling, and small and large polarization. By imposing stationarity of the functional equation (1) with respect to variations of the densities $\rho_\uparrow$ and $\rho_\downarrow$ one obtains a set of coupled Schrödinger-type equations—the KS equations (see Supplementary Information)—of an effective noninteracting system. From the eigenstates and eigenvalues of the KS equations one can compute the density profiles, the ground-state energy and the band structure.

As a first application we consider a repulsive Fermi gas in shallow and moderately deep optical lattices. Repulsive interactions are realized in experiments when the gas is prepared in the excited branch of the Feshbach resonance. We parametrize the interactions by the ratio a/d of the scattering length a and the lattice spacing d, and the density ρ in units of the band filling $n = \rho d^3$. In Fig. 1 we compare KS-LSDA results to direct QMC simulations in an optical lattice. The excellent agreement demonstrates that DFT calculations with a LSDA functional are reliable in weak and moderate optical lattices. To compare HK-LSDA and KS-LSDA, we first show, in Fig. 2, the density of states at half-filling ($n = 1$) in a moderately deep optical lattice with intensity $V_0 = 3E_R$. Here, interactions lead to a partial polarization of the system, seen as a shift between the density of states of the two components: there are more spin-up than spin-down atoms if we fill the system to the Fermi level. The cruder HK-LSDA approximation (green line), on the other hand, predicts zero polarization, and misses the existence of a bandgap that is clearly visible in both the free fermion and KS-LSDA results.

Calculating the ground-state polarization for a range of lattice depths V_0, band fillings n, and interaction strengths a/d we obtain the phase diagrams of Fig. 3. In a shallow lattice with $V_0 = 0.5E_R$ (Fig. 3a) we see three phases: a paramagnetic phase at weak interactions (white), partially polarized (shown as pink gradations), and fully polarized (ferromagnetic, shown in solid red). The phase boundaries in this shallow lattice are similar to those of the homogeneous system $V_0 = 0$ (ref. 16), indicated by the green and blue lines. In deeper optical lattices ($V_0 = 2E_R$ in Fig. 3b and $V_0 = 4E_R$ in Fig. 3c) polarization sets in at much weaker interactions, indicating that the optical lattice strongly favours ferromagnetism.

We can see two prominent features due to the presence of an optical lattice. The first is the much bigger extent of the polarized phases, which is due to the higher local density at the potential minima in the optical lattice and increases the local density beyond the critical value for polarization. Comparing Fig. 3c and d we see that including the accurate kinetic energy in the KS-LSDA this effect is even stronger than in the simpler HK-LSDA approximation. A second striking effect is the non-monotonic behaviour of the phase boundary: there is a large fully polarized region at densities up to half-filling ($n \leq 1$), which rapidly shrinks at higher filling. This phenomenon is due to band structure effects and a gap between up-spin and down-spin subbands. It is thus completely absent in the HK-LSDA approximation (Fig. 3d), which ignores band structure effects.

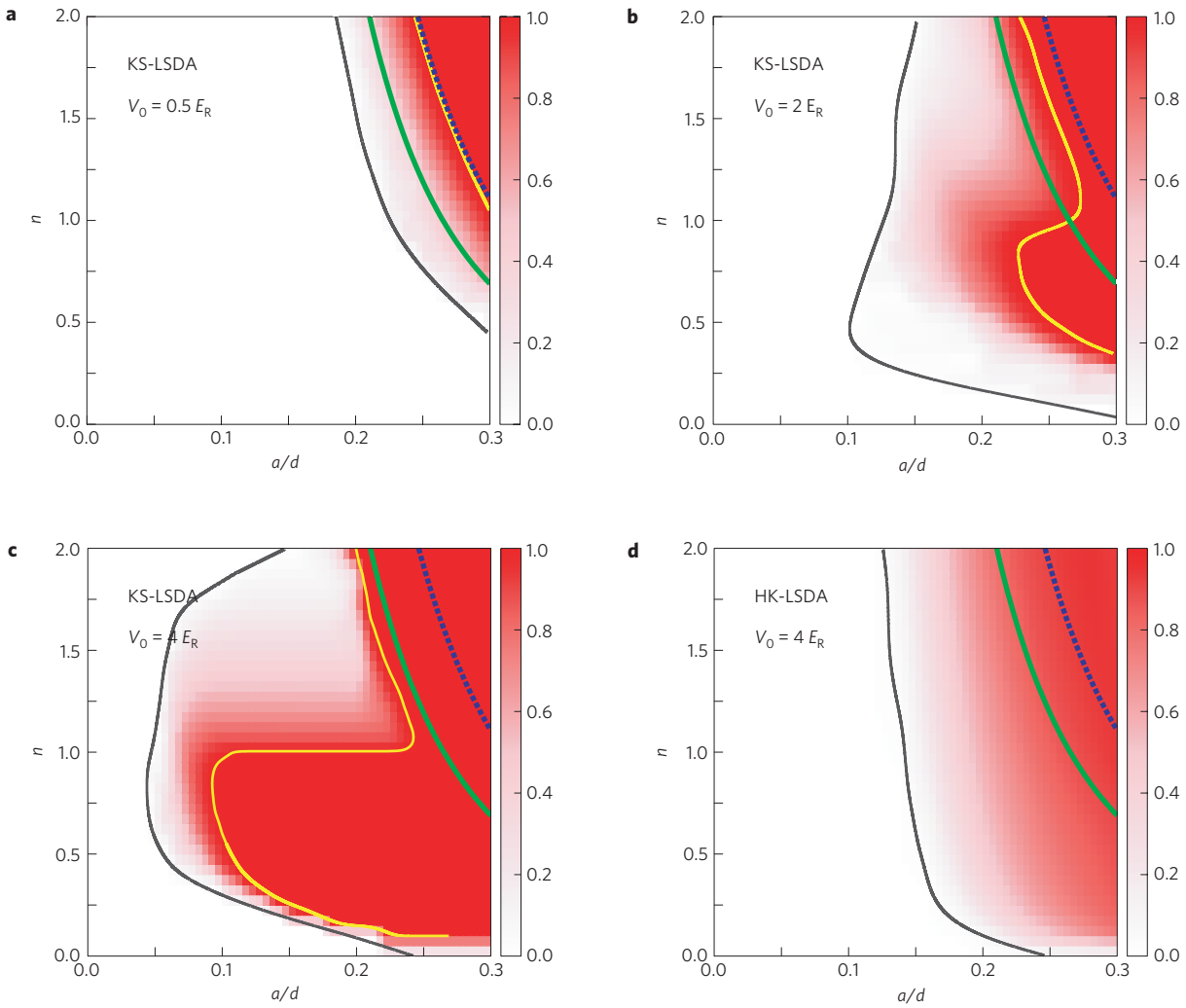

Figure 3 | Phase diagrams at fixed optical lattice intensity V_0. a–c, The red-colour intensity indicates the polarization $P = (\rho_\uparrow - \rho_\downarrow)/(\rho_\uparrow + \rho_\downarrow)$ for optical lattice depths (**a**) $V_0 = 0.5E_R$, (**b**) $V_0 = 2E_R$, (**c**) $V_0 = 4E_R$. **d**, Results for $V_0 = 4E_R$ using HK-LSDA instead of KS-LSDA. The green and blue curves indicate, respectively, the transitions to partially and fully polarized phases in homogeneous systems ($V_0 = 0$). The grey and yellow curves indicate the corresponding transitions in the optical lattice. Ferromagnetism dominates in the region of large optical-lattice intensity V_0 and scattering length a, where a non-trivial phase boundary arises owing to the KS band theory, which cannot be captured using HK-LSDA.

Thus we next calculate the detailed band structure of the interacting system, shown in the left panels of Fig. 4 for a weak optical lattice ($V_0 = 2E_R$) without a bandgap and on the right for a moderate optical lattice with a bandgap ($V_0 = 4E_R$). Weak interactions ($a = 0.04d$) change the band structure only slightly. Increasing the interaction to $a = 0.08d$ (second row) we find a partially polarized state in the deeper lattice: the two spin subbands split and the band structure is substantially changed. At even stronger interaction $a = 0.16d$ (third row) the gas is partially polarized also in the shallower lattice, and becomes fully polarized in the deeper lattice. Note that here the fermions are fully polarized up to half band filling $n = 1$, as only the up-spin subband gets occupied. Notice also that in the fully polarized state the first band is fully occupied and the system is insulating owing to the gap between the first and second subbands. Filling the bands further puts fermions in the next band with opposite spin, resulting in a partially polarized state. This explains the sharp feature around $n = 1$ in the phase diagram in Fig. 3c. To recover full polarization for $n > 1$ one needs to increase either the interaction strength or lattice depth to push the energy of the lowest down-spin subband above the second up-spin subband.

To see antiferromagnetism competing with ferromagnetism at half band filling $n = 1$ we need to consider a unit cell consisting of two lattice sites, and compare the energies of antiferromagnetic and uniform configurations. We find, as shown in Fig. 5, that antiferromagnetic ordering is preferred at intermediate interaction strengths and half band filling, matching with the single band Hubbard model physics, which becomes valid in the upper left-hand corner of the phase diagram shown.

There are many further applications of DFT for atomic gases. Already in this simple system we have seen striking effects, such as substantially enhanced ferromagnetism and strikingly non-monotonic behaviour of the phase boundaries, which is not present in a simple HK-LSDA approximation.

Hybrid functionals, which are successfully used in electronic structure calculations, can be adapted to atomic gases based on our LSDA functional. Examples are Hedin's GW method[18], the LDA+U method[19], which combines LSDA with a Hartree–Fock approximation, and the LDA + DMFT (ref. 20), which combines an LSDA functional with a dynamical mean field theory[21] (DMFT) treatment of the correlated orbitals.

Another extension is functionals for attractive interactions using the local pair density approximation[22], which has been developed

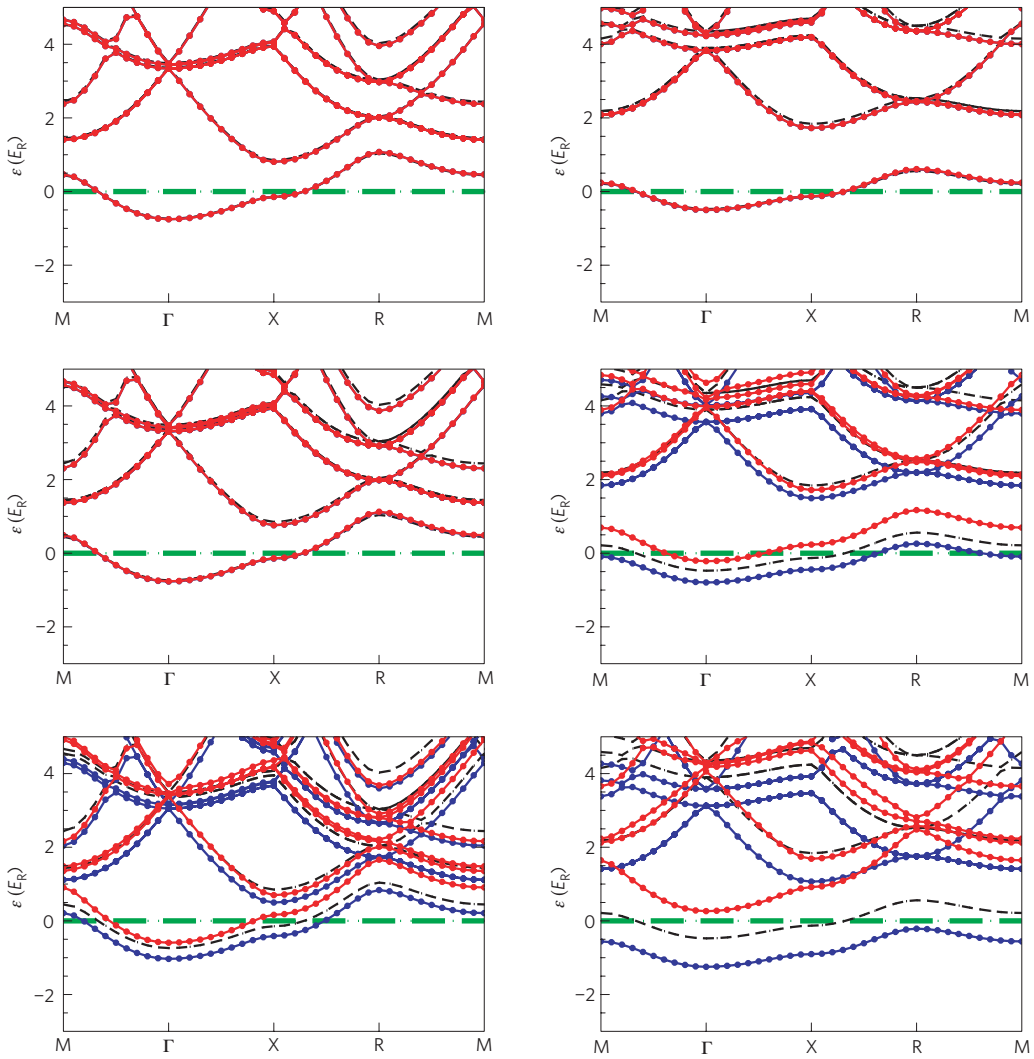

Figure 4 | Band structure. Shown are band structures for two lattice depths, $V_0 = 2E_R$ in the left column and $V_0 = 4E_R$ in the right column, and three values of scattering length ($a = 0.04, 0.08, 0.16\,d$ from top to bottom) at half-filling $n = 1$. The blue and red curves correspond to the majority and minority spin-component respectively. The black curves are the result for an unpolarized noninteracting gas. Energies are given relative to the chemical potential, shown as the dashed green line at 0. The wavevector values given on the x axis scan a curve which goes through the high-symmetry points $\Gamma = (0,0,0)$, $X = (0,\pi/d,0)$, $R = (\pi/d,\pi/d,\pi/d)$ and $M = (\pi/d,\pi/d,0)$ of the first Brillouin zone.

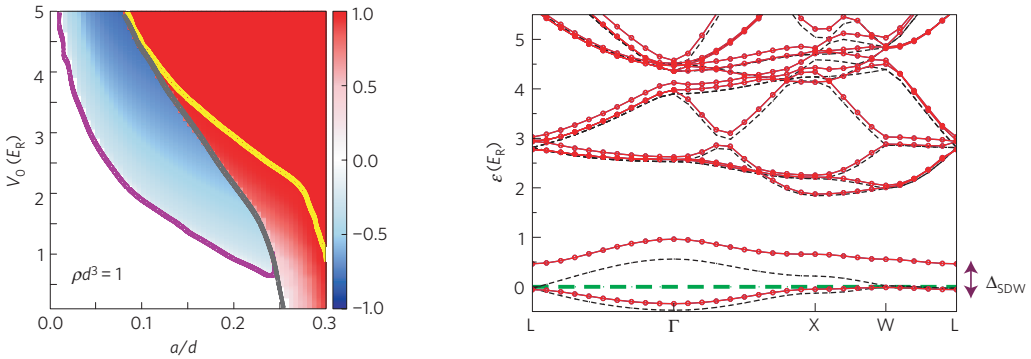

Figure 5 | Phase diagram and antiferromagnetic band structure at half-filling $n = \rho d^3 = 1$. Left: ferromagnetic (antiferromagnetic) phases are indicated by the red-coloured polarization (blue-coloured staggered polarization). As the scattering length a increases, the fermionic optical lattice undergoes phase transitions from an unpolarized to an antiferromagnetic and finally to a ferromagnetic phase. Right: to observe antiferromagnetism, the unit cell has to be doubled, resulting in a face-centred cubic lattice. A spin-density-wave gap Δ_{SDW} shows up in the antiferromagnetic state of an optical lattice with laser intensity $V_0 = 4E_R$ and scattering length $a = 0.08d$. Here, the high symmetry points are $\Gamma = (0,0,0)$, $X = (0,\pi/d,0)$, $L = (\pi/2d,\pi/2d,\pi/2d)$ and $W = (\pi/2d,\pi/d,0)$.

to describe superconducting electronic systems, including not only the fermionic densities $\rho_\uparrow$ and $\rho_\downarrow$ but also a density for paired fermions ρ_p, or the superfluid LDA method of Bulgac[23]. Potentially most useful are generalizations of DFT to finite temperatures[24] (see also refs 25,26 for a recent review) and using time-dependent DFT (ref. 27) to study thermal and non-equilibrium properties of quantum gases.

DFT can thus form an important bridge between atomic physics and materials simulation, much stronger than the Hubbard model, which is at the centre of attention now but relevant only to a small class of materials. Innovations in DFT for materials science provide valuable tools for the investigation of the intriguing physics of quantum gases. In return, atomic gases provide an ideal test bed to address the challenges faced in the simulation of correlated fermionic systems and will help to further improve functionals for strongly correlated systems—thus realizing the promise of optical lattice quantum simulators to be a useful tool for materials science.

Methods

Fermions in an optical lattice. In the presence of an optical field created by three pairs of counter-propagating laser beams, the neutral fermions experience a potential due to dipole-field interaction, that is $V(\mathbf{r}) = \sum_{\alpha=x,y,z} V_0 \sin^2(2\pi r^\alpha/\lambda)$, where λ is the laser wavelength and V_0 the laser intensity, conveniently expressed in units of the recoil energy $E_R = (\hbar^2/2m)(2\pi/\lambda)^2$ ($\hbar$ is the reduced Planck constant and m is the atomic mass). Here, fermions with like spins follow the Pauli exclusion principle and those with unlike spins scatter with the scattering length a, in units of the lattice spacing $d = \lambda/2$.

Solving the KS equations. Owing to cubic translational symmetry, the coupled spin-up and spin-down KS Hamiltonians are diagonalized self-consistently via the Bloch ansatz in a 11^3 plane wave basis, with 20^3 $\mathbf{k}$-points in the first Brillouin zone of the simple cubic lattice. To observe antiferromagnetism, the unit cell has to be doubled, and the doubled unit cells form a face-centred cubic lattice. Details of the KS equations in this basis are presented in the Supplementary Information.

Calculation of the LSDA functional. To determine the LSDA functional we have used the the fixed-node diffusion Monte Carlo method[28] to calculate the ground-state energy of a homogeneous Fermi gas. We simulate a two-component gas with repulsive inter-species interactions (the s-wave scattering between identical particles is inhibited by the Pauli exclusion principle), modelling the interaction by the hard-sphere potential $u(r) = \infty$, if $r < a$, and 0 otherwise. The diameter of the sphere a is equal to the s-wave scattering length. Although this model neglects the effect of the low-energy bound states of the true inter-atomic potential, it represents an improvement with respect to the conventional description of atomic gases in optical lattices, which is based on the Born approximation[14]. The role of non-universal corrections, which depend on details of the potential beyond a, have been analysed in ref. 16 by employing different models with the same scattering length. In the physically relevant regime ($k_F a \lesssim 1$, with a Fermi wave vector $k_F = (3\pi^2\rho)^{1/3}$) these non-universal corrections are very small (<3%). As in previous work[16,29], we fix the nodal surface of the ground-state using a Jastrow–Slater trial wave function, using the Jastrow factor of the exact solution of the two-body problem. The two Slater determinants (one for the spin-up and one for the spin-down particles) are filled with the single-particle eigenstates, namely the plane waves or the Bloch functions (up to the Fermi energy) for simulations in free space or in the optical lattice, respectively. We use up to 81 particles per spin species and up to 6^3 lattice sites, and we find that the finite-size effects are negligible if one follows Fermi liquid theory[30] and includes the finite-size correction terms of a non-interacting Fermi gas.

Received 9 August 2011; accepted 15 May 2012; published online 17 June 2012

References

1. Grosso, G. & Parravicini, G. P. *Solid State Physics* (Academic, 2000).
2. Esslinger, T. Fermi–Hubbard physics with atoms in an optical lattice. *Annu. Rev. Condens. Matter. Phys.* **1,** 129–152 (2010).
3. Hohenberg, P. & Kohn, W. Inhomogeneous electron gas. *Phys. Rev.* **136,** B864–B871 (1964).
4. Kohn, W. & Sham, L. J. Self-consistent equations including exchange and correlation effects. *Phys. Rev.* **140,** A1133–A1138 (1965).
5. Parr, R. G. & Yang, W. *Density-Functional Theory of Atoms and Molecules* (Oxford Univ. Press, 1989).
6. Kohn, W., Becke, A. D. & Parr, R. G. Density functional theory of electronic structure. *J. Phys. Chem.* **100,** 12974–12980 (1996).
7. Chin, C., Grimm, R., Julienne, P. & Tiesinga, E. Feshbach resonances in ultracold gases. *Rev. Mod. Phys.* **82,** 1225–1286 (2010).
8. Joerdens, R., Strohmaier, N., Guenther, K., Moritz, H. & Esslinger, T. A Mott insulator of fermionic atoms in an optical lattice. *Nature* **455,** 204–U34 (2008).
9. Greiner, M., Mandel, O., Esslinger, T., Hansch, T. W. & Bloch, I. Quantum phase transition from a superfluid to a Mott insulator in a gas of ultracold atoms. *Nature* **415,** 39–44 (2002).
10. Gull, E. *et al.* Continuous-time Monte Carlo methods for quantum impurity models. *Rev. Mod. Phys.* **83,** 349–404 (2011).
11. Kozik, E. *et al.* Diagrammatic Monte Carlo for correlated fermions. *Europhys. Lett.* **90,** 10004 (2010).
12. Fuchs, S. *et al.* Thermodynamics of the 3D Hubbard model on approaching the Néel transition. *Phys. Rev. Lett.* **106,** 030401 (2011).
13. Trotzky, S. *et al.* Suppression of the critical temperature for superfluidity near the Mott transition. *Nature Phys.* **6,** 998–1004 (2010).
14. Büchler, H. P. Microscopic derivation of Hubbard parameters for cold atomic gases. *Phys. Rev. Lett.* **104,** 090402 (2010).
15. Jo, G-B. *et al.* Itinerant ferromagnetism in a Fermi gas of ultracold atoms. *Science* **325,** 1521–1524 (2009).
16. Pilati, S., Bertaina, G., Giorgini, S. & Troyer, M. Itinerant ferromagnetism of a repulsive atomic Fermi gas: A quantum Monte Carlo study. *Phys. Rev. Lett.* **105,** 030405 (2010).
17. Ceperley, D. M. & Alder, B. J. Ground state of the electron gas by a stochastic method. *Phys. Rev. Lett.* **45,** 566–569 (1980).
18. Hedin, L. New method for calculating one-particle Green's function with application to the electron-gas problem. *Phys. Rev.* **139,** A796–A823 (1965).
19. Anisimov, V. I., Aryasetiawan, F. & Lichtenstein, A. I. First-principles calculations of the electronic structure and spectra of strongly correlated systems: The LDA+U method. *J. Phys.* **9,** 767–808 (1997).
20. Kotliar, G. *et al.* Electronic structure calculations with dynamical mean-field theory. *Rev. Mod. Phys.* **78,** 865–951 (2006).
21. Georges, A., Kotliar, G., Krauth, W. & Rozenberg, M. J. Dynamical mean-field theory of strongly correlated fermion systems and the limit of infinite dimensions. *Rev. Mod. Phys.* **68,** 13–125 (1996).
22. Oliveira, L. N., Gross, E. K. U. & Kohn, W. Density-functional theory for superconductors. *Phys. Rev. Lett.* **60,** 2430–2433 (1988).
23. Bulgac, A. Local-density-functional theory for superfluid fermionic systems: The unitary gas. *Phys. Rev. A* **76,** 040502 (2007).
24. Mermin, N. D. Thermal properties of the inhomogeneous electron gas. *Phys. Rev.* **137,** A1441 (1965).
25. Argaman, N. & Band, Y. B. Finite-temperature density-functional theory of Bose–Einstein condensates. *Phys. Rev. A* **83,** 023612 (2011).
26. Prodan, E. Raising the temperature on density-functional theory. *Physics* **3,** 99 (2010).
27. Marques, M. A. L. (ed.) *Time-Dependent Density Functional Theory* (Lecture Notes in Physics, Springer, 2006).
28. Reynolds, P. J. *et al.* Fixed-node quantum Monte Carlo for molecules. *J. Phys. Chem.* **77,** 5593–5603 (1982).
29. Lobo, C., Recati, A., Giorgini, S. & Stringari, S. Normal state of a polarized Fermi gas at unitarity. *Phys. Rev. Lett.* **97,** 200403 (2006).
30. Lin, C., Zong, F. H. & Ceperley, D. M. Twist-averaged boundary conditions in continuum quantum Monte Carlo algorithms. *Phys. Rev. E* **64,** 016702 (2001).

Acknowledgements

We acknowledge useful discussions with J. Hutter, L. Pollet, T. Schulthess and J. van de Vondele. This work was supported by the Swiss National Science Foundation, the National Competence Centers in Research (NCCRs) 'Materials with Novel Electronic Properties' (MaNEP) and 'Quantum Science and Technology' (QSIT) and by a grant from the Army Research Office through the DARPA Optical Lattice Emulator (OLE) program.

Author contributions

M.T. and X.D. developed the DFT for ultracold quantum gases. S.P. performed the quantum Monte Carlo simulations. S.P. and M.T. extracted the LSDA functional. P.N.M. performed the DFT calculations. All authors contributed to writing the manuscript and the results presented.

Additional information

The authors declare no competing financial interests. Supplementary information accompanies this paper on www.nature.com/naturephysics. Reprints and permissions information is available online at www.nature.com/reprints. Correspondence and requests for materials should be addressed to M.T.